JOURNAL OF SPACECRAFT AND ROCKETS
Vol. 46, No. 3, May–June 2009

Coupled Analysis of Flow and Surface Ablation in Carbon–Carbon Rocket Nozzles

Daniele Bianchi,* Francesco Nasuti,† and Emanuele Martelli‡
University of Rome "La Sapienza," 00184 Rome, Italy

DOI: 10.2514/1.40197

A study is conducted to predict carbon–carbon nozzle recession behavior in solid rocket motors for wide variations of propellant formulations and motor operating conditions. The numerical model considers the solution of Reynolds-averaged Navier–Stokes equations in the nozzle, heterogeneous chemical reactions at the nozzle surface, variable transport and thermodynamic properties, and heat conduction in the nozzle material. Results show that the ablation rate is largely determined by the diffusion of the major oxidizing species (H_2O, CO_2, OH) to the nozzle surface. Both the concentration of the major oxidizing species (affected by the aluminum content of the propellant) and the chamber pressure exert a strong influence on the ablation rate: it increases almost linearly with chamber pressure and it decreases with increasing aluminum content of propellants. The calculated results show an excellent agreement with the experimental data from the ballistic test and evaluation system motor firings.

Nomenclature

A	=	cross-section area, m^2
D_{im}	=	effective diffusion coefficient, m^2/s
h	=	enthalpy, J/kg
k	=	thermal conductivity, $W/m \cdot K$
Le	=	Lewis number
M	=	Mach number
$\dot{m}$	=	mass blowing rate per unit area, $kg/m^2 \cdot s$
N_c	=	number of species
N_{el}	=	number of elements
p	=	pressure, N/m^2
r	=	distance from surface, m
$\dot{s}$	=	erosion rate, m/s
T	=	temperature, K
t	=	time, s
u	=	streamwise velocity, m/s
v	=	velocity component normal to surface, m/s
W	=	molecular weight, kg/kmole
Y	=	elemental mass fraction
y	=	mass fraction
y^+	=	dimensionless wall distance
α_{ki}	=	mass fraction of element k in species i
ΔH_{abl}	=	heat of ablation, J/kg
η	=	outward coordinate normal to surface
μ_t	=	turbulent viscosity, $kg/m \cdot s$
ρ	=	density, kg/m^3

Subscripts

c	=	combustion chamber
i	=	species
k	=	element
s	=	solid (carbon) properties at gas–solid interface
t	=	throat
w	=	gas properties at gas–solid interface

Presented as Paper 3912 at the 40th Thermophysics Conference, Seattle, WA, 23–26 June 2008; received 1 August 2008; revision received 19 January 2009; accepted for publication 17 March 2009.

*Research Fellow, Dipartimento Meccanica e Aeronautica, Via Eudossiana 18. Student Member AIAA.

†Associate Professor, Dipartimento Meccanica e Aeronautica, Via Eudossiana 18. Senior Member AIAA.

‡Assistant Professor; currently Second University of Naples, Dipartimento Ingegneria Aerospaziale e Meccanica, Via Roma 29, 81131 Aversa, Italy. Member AIAA.

I. Introduction

WITH the development of high-energy solid propellants and harder firing conditions in advanced solid rocket motors (SRM), carbon–carbon (C/C) materials have found increasing application in SRM nozzles because of their excellent thermal and physical properties and low densities. But in spite of these advantages, the C/C nozzle surface recedes because of the chemical attack by the exhaust gases increasing the nozzle throat area and resulting in a nominal performance loss. The identification and description of the major mechanisms governing the nozzle erosion has been the subject of many investigations [1–10] in solid rocket technology. The models developed to predict the nozzle erosion in the 1960s and 1970s, when limited computational resources were available, included necessarily simplifying assumptions because a complete model should take into account numerous parameters: solid-propellant composition, motor operating conditions, duration of firing, nozzle geometry and material properties, geometric and thermal history of the nozzle, rates of diffusion of the species through the boundary layer, and heterogeneous chemical reactions with the surface material.

Erosion is a direct consequence of the fact that, as the propellant of the rocket motor burns, the C/C nozzle wall is exposed to the hot exhaust gas and its surface temperature increases. At high surface temperatures, heterogeneous chemical reactions begin to occur between the nozzle material and the oxidizing species present in the exhaust gas, resulting in the thermochemical erosion of the nozzle. Many researchers [1,7–12] have concluded that the most reactive gases are those that react with carbon to form carbon monoxide, such as H_2O, CO_2, and OH, normally found in a significant amount in the exhaust gas. In particular, Swope and Berard [1] found a direct correlation between the nozzle erosion and the total concentration of the oxidizers capable of forming CO with the graphite and showed that H_2O is the major contributor to nozzle erosion. Heterogeneous reactions consume the oxidizing species at the nozzle surface and thereby create species concentration gradients in the boundary layer that result in the diffusion of oxidizing species to the nozzle surface. Thus, the erosion rate will depend on both the diffusion rate of oxidizing species across the boundary layer to the wall and on the chemical kinetic rates of heterogeneous reaction at the surface, as shown by a simple model for the erosion of graphite throat nozzles developed by Delaney et al. [2]. The lowest rate process will control

the rate of the overall nozzle erosion: if the kinetic rates are much higher than the diffusion rates, the recession rate is governed by the diffusion mechanism of oxidizing species (diffusion-limited erosion). The other extreme situation is that of high diffusion rates and low kinetic rates, in which case the recession is determined by the chemical kinetics (kinetic-limited erosion). Concerning this aspect, McDonald and Hedman [4], on the basis of the results of an analytical study and analysis of short-duration test data, found that the erosion of graphite is kinetic limited during the transiently heated period, and diffusion limited when surface temperature exceeds about 2000 K. Finally, some material may be lost by sublimation of the graphite itself as pointed out by Klager [7] even if sublimation can be considered of minor importance as an ablation mechanism because SRM nozzles presently operate at temperatures too low to activate oxidation/sublimation transition. In addition to the aero-thermochemical processes, the erosion may have contributions from the mechanical processes caused by impact of condensed metal-oxide particles (e.g., Al_2O_3) on the nozzle surface or by structural failure because of high thermal stresses. However, it has been shown that the chemical erosion is the primary reason for the nozzle recession [2–4,7,11]. For instance, Geisler [11] used a BATES (ballistic test and evaluation system) motor to measure the recession rate as a function of aluminum content of the propellant and found that the recession rate was proportional to the concentration of H_2O, OH, and CO_2 and decreased as the propellant aluminum content was increased, thus showing that alumina particle impingement is not an important erosion mechanism. Further studies have demonstrated that erosion rate is not related to the flame temperature. In particular, Klager [7] found, on the basis of data obtained by experimental firings on small aluminized SRM, that erosion depended primarily on pressure and on chemical attack by H_2O and CO_2 whereas the flame temperature showed poor correlation with the recession rate. Most of the preceding findings were confirmed by the theoretical studies of Kuo and Keswani [8], Keswani and Kuo [9], and Keswani et al. [13] who showed that, in a wide range of propellant formulations and operating pressures and temperatures, recession is strongly influenced by propellant composition and chamber pressure whereas the influence of chemical kinetics is predominant only at low surface temperatures (below about 2500 K).

The objective of this study is to formulate and to validate a comprehensive model based on a full Navier–Stokes approach coupled with a thermochemical equilibrium ablation model for predicting the erosion rate of C/C SRM nozzles and to study the effect of motor operating conditions and propellant formulation on the erosion process. In particular, in the present paper heterogeneous chemical reactions at the nozzle surface, rate of diffusion of the species through the boundary-layer, heat conduction inside the C/C material, and variable multispecies thermophysical properties are taken into account. To the authors knowledge, only another approach to solve Navier–Stokes equations with coupled ablation for SRM nozzle erosion analysis can be found in the literature [12]. Yet that approach, recently published, is different from the present approach because of the numerical scheme adopted, the turbulence model, and the surface thermochemistry model (it considers finite-rate chemistry compared with the present chemical equilibrium approach).

II. Theoretical Modeling

In the present formulation the gas-phase dynamics are based on the full Navier–Stokes equations for single-phase multicomponent reacting systems where variable thermodynamic and transport properties are accounted for. The heat conduction process in the nozzle is treated as being 1-D and steady state.

A. Governing Equations for the Gas Phase

The governing equations for the gas phase are the reacting turbulent Reynolds-averaged Navier–Stokes equations written for 2-D axisymmetric flows. For the present study it is only important to stress that the two following major assumptions are made: 1) radiation heat transfer is negligible, and 2) gas-phase reactions have a negligible effect on the recession process (frozen flow in the gas phase).

The first assumption is made because radiation is usually one order of magnitude less than convection in rocket nozzle applications [8,10]. The second assumption is justified by literature studies[9,12] showing that the graphite recession process is relatively independent of gas-phase reactions.

B. Governing Equations for the Solid Phase

The heat conduction in the solid material is an important mechanism that has to be considered in the recession analysis [8,12,14]. It is assumed that heat conduction into the C/C material is dominant in the radial direction. In a moving local coordinate system tied to the receding surface, the temperature distribution at a given distance r from the surface is governed by the following equation [14,15]:

$$\rho_s \frac{\partial h_s}{\partial t} = \frac{1}{A}\frac{\partial}{\partial r}\left(k_s A \frac{\partial T_s}{\partial r}\right) + \rho_s \dot{s}\frac{\partial h_s}{\partial r} \tag{1}$$

The terms in Eq. (1) represent, from left to right, the sensible energy accumulation, the net conduction, and the net energy convected as a consequence of coordinate motion. A closed-form solution of the heat conduction equation at a steady state [16,17] is available integrating Eq. (1) between the nozzle–gas interface and the nozzle outer wall assuming an adiabatic condition for the latter and a steady-state condition ($\partial \cdot / \partial t = 0$). This approximation is made in the present study because the heating of the C/C in the SRM environment is very quick [8,18]: the surface temperature reaches 2000–2500 K in less than 1 s of exposure and then increases very slowly with time, denoting an almost steady-state condition.

C. Gas–Surface Boundary Conditions

Because of the chemically active surface, further physical modeling is necessary for the gas–surface interaction. To complete the formulation of the theoretical model, boundary conditions must be specified at the gas–solid interface, which describes the physics of the surface phenomena.

Consider the fluxes of mass/energy entering and leaving a control surface fixed to the ablating surface. The graphite surface material may be visualized as moving into the surface at a rate $\dot{s} = \dot{m}/\rho_s$. If it is assumed that no material is being removed in a condensed phase (solid or liquid), then the general surface mass/energy balances for a chemically reacting, graphitic ablating surface can be written as [17]

$$\rho D_{im}\left.\frac{\partial y_i}{\partial \eta}\right|_w + \dot{m}_i = (\rho v)_w y_{i_w} \qquad i = 1, N_c \tag{2}$$

which is the surface mass balance (SMB) for the ith species, and

$$k\left.\frac{\partial T}{\partial \eta}\right|_w + \sum_i^{N_c} h_{i_w}\rho D_{im}\left.\frac{\partial y_i}{\partial \eta}\right|_w + \dot{m}h_s = (\rho v)_w h_w - k_s\left.\frac{\partial T_s}{\partial r}\right|_s \tag{3}$$

which is the surface energy balance.

The terms on the left-hand side of Eq. (2) are the mass fluxes of species i entering the surface due to diffusion and heterogeneous surface reactions, respectively, whereas the term on the right-hand side is the mass flux of species i leaving the surface due to surface ablation. The source term $\dot{m}_i$ is positive for the ablation products and negative for the oxidizing species, which are consumed in the ablation process.

The terms on the left-hand side of Eq. (3) are the heat fluxes entering the surface due to conduction from gas, diffusion, and surface motion, respectively, whereas the terms of the right-hand side are the heat fluxes leaving the surface due to surface ablation and conduction in the material. The conduction term $-k_s \partial T_s/\partial r$ is represented by a closed expression available at a steady state from Eq. (1). Thus, the solid- and gas-phase boundaries are coupled at the interface.

A summation of Eq. (2) over all the species yields the total mass rate

$$\sum_i \dot{m}_i = (\rho v)_w = \dot{m} = \rho_s \dot{s} \tag{4}$$

Now introducing in Eq. (2) the variable $y_{i_s} = \dot{m}_i/\dot{m}$, which is the mass of species i produced or consumed in the ablation process per mass of TPS (thermal protection systems) material ablated, and substituting Eq. (2) into Eq. (3), yields a compact form of the surface energy balance:

$$k \left.\frac{\partial T}{\partial \eta}\right|_w - \dot{m}\Delta H_{\text{abl}} = -k_s \left.\frac{\partial T_s}{\partial r}\right|_s \tag{5}$$

The term $\Delta H_{\text{abl}} = (\sum_i h_{i_w} y_{i_s} - h_s)$ is the so-called heat of ablation, which is the difference between the enthalpies of the species created or consumed by the ablation process and the enthalpy of the solid material at the surface temperature per mass of material removed; hence the term $-\dot{m}\Delta H_{\text{abl}}$ represents the heat flux absorbed (when negative) by the thermochemical ablation process, which will be referred to as *chemical heat flux*.

It has been found [4,8,9] that the erosion is kinetic controlled when surface temperature is below 2000–2500 K. Above this transition temperature, which is highly dependent on the chemical kinetics [12] and sometimes can be as high as 2800 K [12], the chemical reactions become sufficiently fast to consume all the oxidizing species diffusing to the surface and local chemical equilibrium is established at the solid–gas interface. When such a condition is reached, the erosion process is considered diffusion limited and the solution is not dependent on the kinetic rates of the heterogeneous surface reactions. Calculations presented in [8,18] have shown that, for typical metallized propellant in SRM, the surface temperature in the throat region exceeds 2000–2500 K after a second or less from ignition so that the nozzle erosion is essentially diffusion-controlled during the whole operational duration. For this reason, a surface equilibrium assumption is considered appropriate, as long as the calculated surface temperature is above ≈2500 K. Usually such a wall temperature is exceeded for metallized propellants whereas for nonmetallized propellants, which have lower flame temperatures, the surface temperature can fall below this value and chemical kinetic rates may control the recession process [12,14]. In such a case, the diffusion-limited calculations would overestimate the erosion rate. Therefore, a full nonequilibrium model is required for the most general case, which needs the knowledge of the controlling reactions as well as their rate constants. Nevertheless, it has to be kept in mind that a recent study [14] has shown that the prediction of erosion rate is sensitive to the kinetic model adopted. On the contrary, to calculate the equilibrium state of a chemical system, information relative to all chemical reactions is not needed, and a significant simplification in the problem formulation is obtained. Because of this significant simplification and of its validity in most of the applications of interest, the surface equilibrium assumption is made in the present study.

Within the assumption of surface equilibrium it is convenient to express the SMB in terms of the elemental mass fractions Y_k, which are known for the TPS material and unknown at the gas–surface interface. A weighted summation of Eq. (2) over all the species yields a balance equation for each element k:

$$\sum_i \alpha_{ki} \rho D_{im} \left.\frac{\partial y_i}{\partial \eta}\right|_w = \dot{m}(Y_{k_w} - Y_{k_s}) \quad \text{where } Y_{k_s} = \dot{m}_k/\dot{m}$$
$$k = 1, N_{\text{el}} \tag{6}$$

The term Y_{k_s} is the mass of element k produced in the ablation process per mass of TPS material ablated and must be equal to the elemental composition of the TPS material. The use of Eq. (6) together with the assumption of chemical equilibrium at wall permits to bypass the entire discussion about the reaction mechanisms and the associated reaction rates, especially for the complex flowfields with ablation. The surface equilibrium approach provides, in most cases, satisfactory accuracy with reduced computational cost and can account for both oxidation and sublimation of carbon.

The other boundary conditions at the solid–gas interface are

$$u = 0, \qquad v = \dot{m}/\rho, \qquad \partial p/\partial \eta|_w = 0 \tag{7}$$

Solving the surface energy and mass balances, Eqs. (5) and (6), permits to evaluate the ablation mass rate and the surface temperature.

III. Numerical Procedure

The analysis of the SRM nozzle flowfield is performed by a 2-D axisymmetric time-accurate multispecies Reynolds-averaged Navier–Stokes solver [19–21]. The thermodynamic properties for individual species are approximated by seventh-order polynomials of temperature whereas the transport properties are approximated by fourth-order polynomials [22]. Mixture properties for conductivity and viscosity are derived from the Wilke's rule. The diffusion model is based on an effective diffusion coefficient obtained assuming a constant Lewis number. The Spalart–Allmaras one-equation model [23] is used to compute the turbulent viscosity μ_t. Turbulent conductivity and turbulent mass diffusivity are computed from μ_t, specific heat at constant pressure, turbulent Prandtl number (a standard value of 0.9 is assumed), and turbulent Schmidt number (a standard value of 0.9 is assumed). All computations are made considering bulk graphite ($\rho_s = 1.83$ g/cm^3) as the nozzle material, for which thermodynamic properties as a function of temperature are taken from literature data [22]. Assuming surface equilibrium, the chemical composition at the nozzle wall (y_{i_w}) can be obtained using a free energy minimization procedure [22]. The ablation mass rate is then computed from the elemental mass balance Eq. (6) and the surface chemical composition. Once the ablation mass rate has been computed, the erosion rate can be easily derived from Eq. (4) obtaining $\dot{s} = \dot{m}/\rho_s$. The surface temperature is computed from the surface energy balance Eq. (5) using the Newton's iterative procedure. At each CFD (computational fluid dynamics) iteration, the surface temperature, the mass blowing rate, and the wall chemical composition are continuously updated until a steady-state condition is reached.

The computational domain is defined by the nozzle geometry. The nozzle is characterized by subsonic inflow boundary conditions describing the combustion chamber (total temperature and total pressure are enforced together with the flow direction and chemical composition), supersonic outflow, symmetry axis, and solid wall. The inlet flow is a mixture of gases derived from chemical equilibrium calculations.

IV. Results and Discussion

The model described in the preceding sections is implemented to simulate the nozzle erosion in practical solid rocket motor environments. The nozzle geometry employed is similar to the that used in the BATES rocket motor [24] (Fig. 1). In particular, as the exact nozzle geometry is not available in the open literature, it has been rebuilt on the basis of the main geometric parameters (throat radius, overall dimensions, and divergence angle) reported in [24].

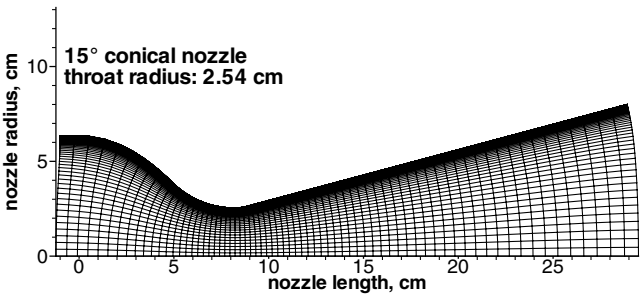

Fig. 1 Rocket nozzle configuration.

Table 1 Nozzle inlet flow conditions

Species	Mass fractions, AP/HTPB/Al	Mass fractions, AP/HTPB
CO	0.23	0.11
CO_2	0.02	0.22
HCl	0.20	0.267
H_2	0.01	0.003
H_2O	0.09	0.29
N_2	0.10	0.10
OH	0.01	0.01
Al_2O_3	0.34	-
Motor conditions		
T_0, K	3500	3000
p_0, bar	69	69

The present nozzle material (bulk graphite) is the same as for the BATES nozzle erosion tests.

The hot exhaust gas flowing in the nozzle consists of the combustion products of a typical metallized and nonmetallized AP/HTPB (ammonium perchlorate/hydroxyl-terminated polybutadiene) composite propellant [12], of which mass fractions are shown in Table 1. These mass fractions have been determined by chemical equilibrium calculations at a chamber pressure of 69 bar. The three oxidizing species considered are H_2O, CO_2, and OH. Other oxidizing species (such as NO, O, and O_2) have not been considered having a much lower mass fraction and, hence, a negligible influence on the recession process. Five values of chamber pressures (49, 59, 69, 79, 89 bar) have been used to study the effect of motor operating parameters, together with a single value of chamber temperature (3000 K for nonmetallized and 3500 K for metallized propellant). Indeed chamber temperature shows only a slight variation with chamber pressure. The mass fractions of all the species remain almost constant with increasing/decreasing chamber pressure with the exception of OH, which has a mass fraction showing some variation. It can be noted (Table 1) that the exhaust gas equilibrium composition changes noticeably when aluminum is added to the propellant: this is because aluminum consumes most of the oxygen in

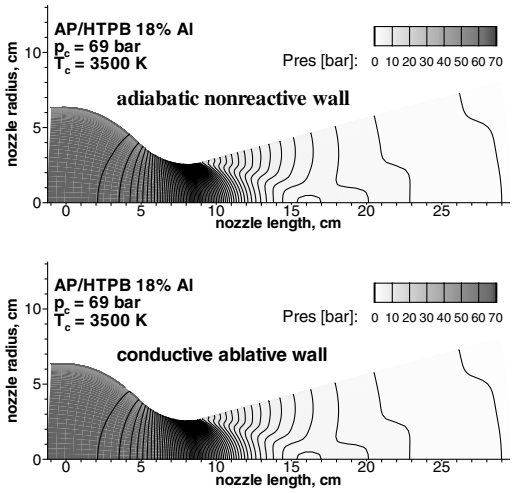

a) Flowfield pressure distribution

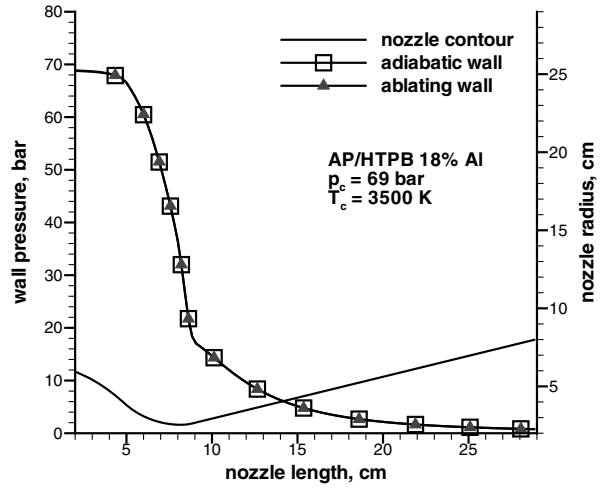

b) Wall pressure distribution

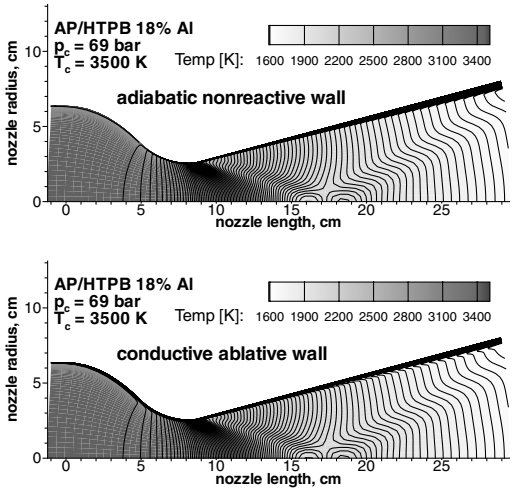

c) Flowfield temperature distribution

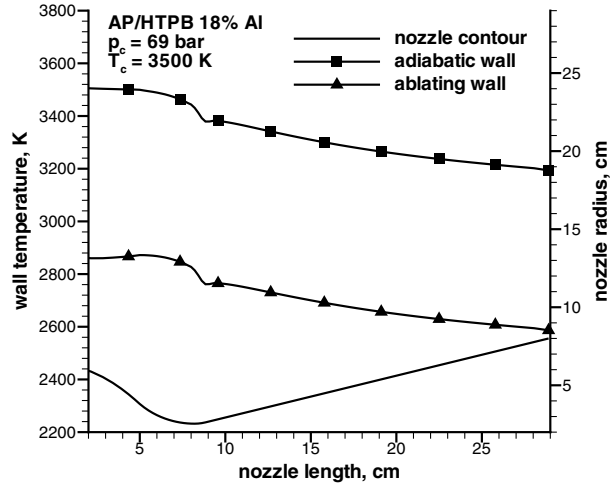

d) Wall temperature distribution

Fig. 2 Adiabatic nonreactive vs conductive ablative wall condition (AP/HTPB/Al, $p_c = 69$ bar, $T_c = 3500$ K).

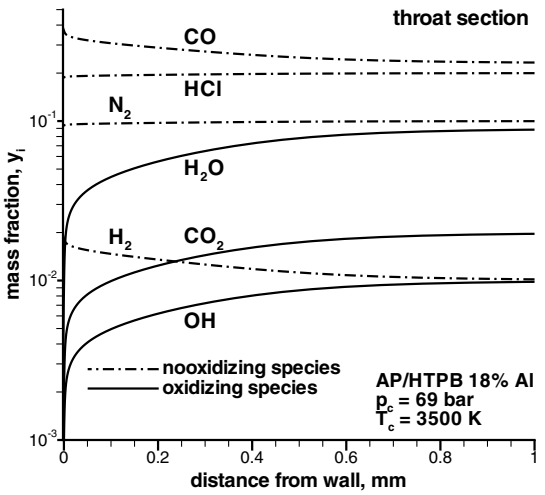

a) Distribution of species in the boundary layer at nozzle throat

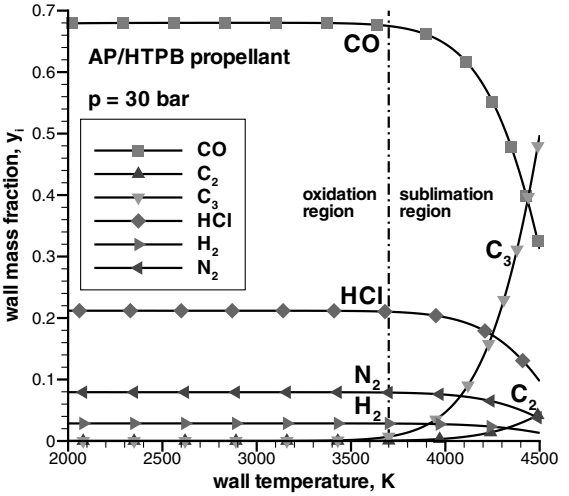

b) Wall equilibrium composition vs wall temperature at throat pressure

Fig. 3 Distribution of species inside the boundary layer at throat and chemical equilibrium composition.

the propellant to form Al_2O_3 and other oxides of aluminum. Thus, a lower amount of oxidizing species (H_2O, CO_2, and OH) is available in the exhaust gas. The outside nozzle wall temperature is 300 K for all computations. A single-phase treatment is used in the model so that all the Al_2O_3 present in the exhaust gas of metallized propellants is assumed to be in the gas phase. The computational domain is subdivided into 60×70 grid points in the axial and radial directions, respectively (Fig. 1). In the r direction, meshes are clustered near the nozzle surface such to ensure a value of y^+ less than 1.0 all along the nozzle length to accurately capture the near-wall phenomena. All the computations presented are at a steady-state condition, and a grid sensitivity analysis has been carried out to ensure that results are grid independent.

A. Analysis of Results

The results obtained with the present approach for the case of $p_c = 69$ bar, $T_c = 3500$ K with metallized AP/HTPB/Al propellant are shown in Fig. 2, where the pressure and temperature contours and wall distributions are compared with those obtained considering a reference test case with a nonreactive adiabatic wall. Results obtained with the ablative boundary conditions show almost no differences in the core-flow region with the adiabatic nonreactive computations (Fig. 2a and 2c). The main differences are experienced in the boundary layer and at the nozzle surface: therefore our attention will be directed toward the boundary-layer structure with ablation. The wall pressure distribution in Fig. 2b is unaffected by the ablation process whereas the difference between the two temperature distributions in Fig. 2d is significant: wall temperature is lower in the case of ablation. This effect is mainly due to the endothermic surface heterogeneous reactions (which consumes CO_2, OH, and H_2O to form CO and H_2), but it is also enhanced by the fact that the wall is made conductive, with part of the incoming heat flux being transferred to the solid material. The knee visible in the wall temperature distribution is due to the change of curvature between the throat and the conical divergent section of the nozzle.

Figure 3a shows the species distribution in the boundary layer at the throat section ($p_t = 30$ bar, $T_t = 2800$ K). The oxidizing species are shown by solid lines, whereas nonoxidizing are represented by dashed lines. Examining the distribution of oxidizing species, several interesting observations can be made. First, it is clear that H_2O is by far the dominant oxidizing species, as CO_2 and OH, the next important oxidizing species, have a mass fraction of about one order of magnitude lower. Second, because the nozzle erosion is diffusion controlled, the mass fraction of these oxidizing species is vanishing small at the nozzle surface.

The analysis of the nonoxidizing species (dashed lines in Fig. 3a) suggests the following comments. First, the mass fractions of CO and H_2 are maximum at the wall because they are produced by the heterogeneous reactions at the surface. Second, N_2 and HCl do not participate in heterogeneous reactions, and hence their mass fractions are nearly constant in the boundary layer, with a slight decrease near the surface because of mass blowing effect. Finally, almost all the oxygen and carbon at the nozzle surface exist as CO because the chemical equilibrium forces all the available oxidizing species at the surface to be entirely consumed. This behavior can be better understood by the analysis of Fig. 3b, which shows the surface equilibrium composition at the throat pressure, plotted as a function of surface temperature. The oxidizing species (CO_2, H_2O, OH) do not appear because they react completely with the solid carbon to form carbon monoxide, so that their mass fraction at wall is vanishing small. For a wide range of surface temperature, namely the oxidation region, one can see that the only ablation product is represented by the species CO and H_2. At high surface temperatures, sublimation is activated and carbonaceous gaseous species such as C_3 and C_2 are produced at a high extent. The effect of surface pressure, not shown, is to shift the curves to the right for increasing pressures and to the left for decreasing pressures. Even at reduced pressures, where sublimation is favored, it is unlikely that an appreciable amount of material would be lost by sublimation because the surface temperature is usually too low to activate this process. As wall temperature at throat is lower than 3500 K, and pressure is relatively high ($\approx$30 bar), the computed composition reported in Fig. 3a shows no production at all of C_3 at the throat.

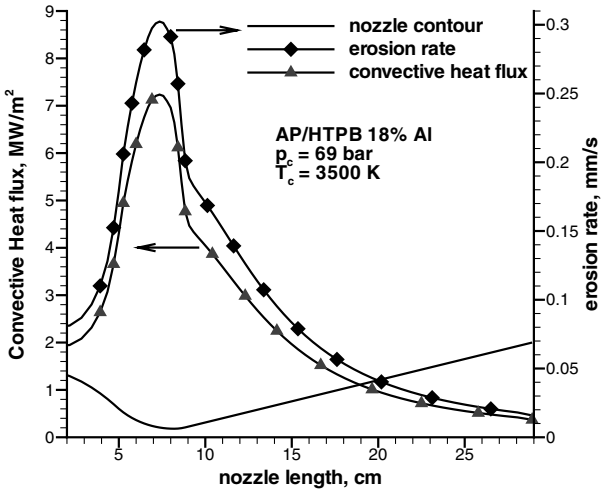

Fig. 4 Erosion rate and convective heat flux distribution (AP/HTPB/Al, $p_c = 69$ bar, $T_c = 3500$ K).

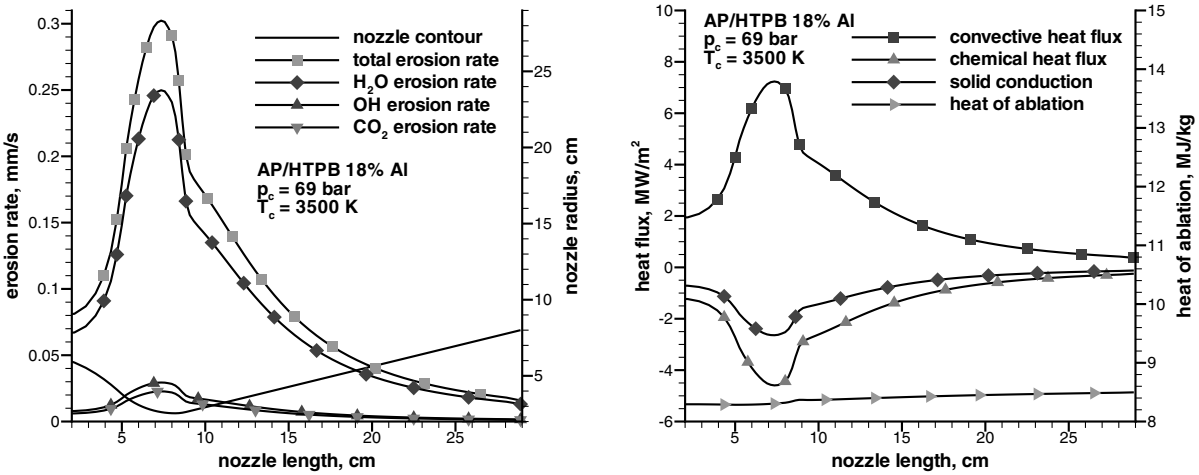

a) Erosion contribution from the three oxidizing species

b) Heat fluxes distribution and heat of ablation along nozzle wall

Fig. 5 Erosion contribution from the oxidizing species and wall heat fluxes (AP/HTPB/Al, $p_c = 69$ bar, $T_c = 3500$ K).

The distribution of the thermochemical erosion rate and the surface convective heat flux along the nozzle length is shown in Fig. 4. It can be noted that the erosion rate is maximum a bit ahead of the throat. Figure 4 clearly shows that the erosion rate distribution follows the same trend as the convective heat flux distribution all along the nozzle wall indicating a direct correlation between the two [8,10,12]: recession and heat flux increase in the converging section of the nozzle, reach a maximum close to the throat, and decrease in the supersonic divergent section.

Figure 5a shows the contributions to the net erosion rate due to the three main oxidizing species. Considering the following three heterogeneous oxidizing reactions:

$$\mathrm{C}_{(s)} + \mathrm{H_2O} \rightleftharpoons \mathrm{CO} + \mathrm{H_2} \qquad \mathrm{C}_{(s)} + \mathrm{OH} \rightleftharpoons \mathrm{CO} + \mathrm{H}$$
$$\mathrm{C}_{(s)} + \mathrm{CO_2} \rightleftharpoons 2\mathrm{CO} \tag{8}$$

It can be seen that a single mole of solid carbon $\mathrm{C}_{(s)}$ can be consumed either with a mole of $\mathrm{H_2O}$, or OH, or $\mathrm{CO_2}$. Hence, the erosion rate contribution due to each oxidizing species can be obtained by a mass conservation equation considering that each oxidizing species is completely consumed at the surface (diffusion-limited regime):

$$\dot{s}_i = \frac{1}{\rho_s}\frac{W_s}{W_i}\left(\rho D_{im}\frac{\partial y_i}{\partial \eta}\bigg|_w\right) \quad \text{with} \quad \dot{s}_{\mathrm{H_2O}} + \dot{s}_{\mathrm{OH}} + \dot{s}_{\mathrm{CO_2}} = \dot{s} \tag{9}$$

The most important oxidizing species is by far $\mathrm{H_2O}$ followed by OH and $\mathrm{CO_2}$ in that order (Fig. 5a), which confirms both theoretical [8–10,12] and experimental results [7,11,25]. Note that, although $\mathrm{CO_2}$ has a larger mass fraction than OH in the exhaust gas, it yields a lower contribution to erosion due to its higher molecular weight.

Figure 5b shows the various heat flux contributions along the nozzle length together with the heat of ablation. Because the surface energy balance is imposed at wall, the sum of the various heat flux contributions is zero. The chemical heat flux is negative all along the nozzle length because the oxidation of carbon in SRM environment is endothermic. A big part of the incoming convective heat flux is absorbed by the endothermic ablation process and the remaining part is conducted into the material. The conductive and chemical heat fluxes show a sharp decrease after the nozzle throat due to the sudden decrease of the convective heat flux and consequently of the erosion mass rate. The heat of ablation remains almost constant along the nozzle length, showing only a variation by few percents. This is because the gas composition at wall is almost constant along the nozzle length, with the only ablation product being carbon monoxide. There is only a slight effect of surface temperature on the heat of ablation: a lower heat of ablation is experienced where surface temperature is higher.

B. Validation by BATES Motor Experimental Data

To validate the current model, calculated recession rates have been compared with the BATES motor experimental data from Geisler [11] and Geisler and Beckman [24]. The BATES motor was developed in the early 1960s and was intensively used to analyze SRM carbon nozzle erosion resulting in many experimental tests and correlations of throat recession as a function of propellant composition and firing condition [24]. Five different propellant compositions have been considered for wide variations of aluminum content and flame temperature (Table 2). The experimental data by Geisler were based on the total throat recession as a function of the burning time (less than 5 s) using a highly amplified and filtered thrust over pressure ratio (F/p) plot to estimate real-time throat diameters. Measured data show that after a transient between 1 and 2 s (during which the carbon heats up), where no erosion has been observed, the erosion increases linearly with time, denoting a steady-state condition and thus permitting to evaluate the erosion rate at the throat for the various propellant formulations.

The computed erosion rate distributions along the nozzle length as a function of the aluminum content of the propellant are plotted in Fig. 6 together with the experimental data measured at the throat. The comparison between the experimental and the computed erosion rates at the throat, which is also reported in Table 3, shows an excellent agreement except for the propellant with the minimum aluminum content. This behavior can be explained by analyzing the surface temperature distributions. The calculated surface temperature (Fig. 7)

Table 2 Mass fractions, pressure, temperature, and aluminum content for validation of experiments by Geisler [25]

y_{CO}	$y_{\mathrm{CO_2}}$	y_{HCl}	$y_{\mathrm{H_2}}$	$y_{\mathrm{H_2O}}$	$y_{\mathrm{N_2}}$	$y_{\mathrm{Al_2O_3}}$	p_c, bar	T_c, K	Al%
0.175	0.04	0.24	0.02	0.145	0.10	0.28	69	3580	15%
0.18	0.025	0.23	0.02	0.105	0.10	0.34	69	3655	18%
0.20	0.015	0.195	0.02	0.07	0.10	0.40	69	3715	21%
0.20	0.005	0.190	0.02	0.045	0.10	0.44	69	3750	24%
0.20	0.005	0.190	0.02	0.025	0.10	0.46	69	3745	27%

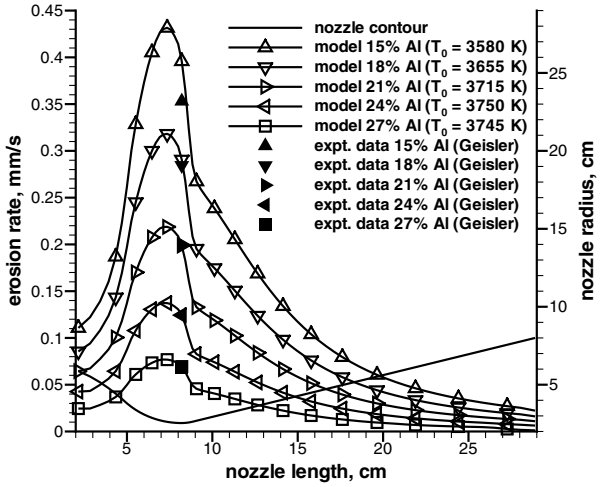

Fig. 6 Erosion rate distribution for propellants with different aluminum content. Experimental data (expt. data) are from [25].

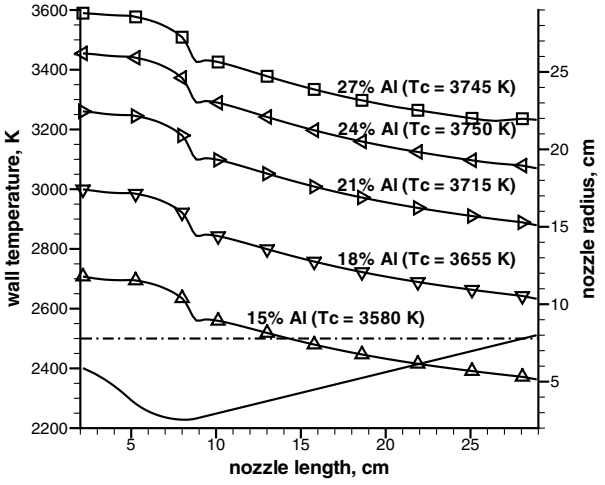

Fig. 7 Wall temperature distribution for propellants with different aluminum content.

is higher for propellant with higher aluminum content due to the combined effect of higher flame temperature and lower erosion rate (lower heat absorption due to endothermic surface reactions). In fact, the recession rate decreases sharply with increasing aluminum content of propellant (Fig. 6) even though the flame temperature

Table 3 Comparison between calculated and experimental data for throat recession

Al%	$\dot{s}_{\text{expt}}$, mm/s	$\dot{s}_{\text{model}}$, mm/s	error%
15%	0.353	0.396	12%
18%	0.284	0.291	2.5%
21%	0.200	0.199	<1%
24%	0.124	0.124	<1%
27%	0.069	0.069	<1%

increases as shown in Table 2. This is because aluminum consumes most of the oxygen in the metallized propellant to form Al_2O_3. Therefore, the graphite erosion cannot be related directly to the chamber temperature. To confirm this, the flame temperature of the 27% Al propellant (Table 2) has been artificially reduced from 3745 K to a much lower value of 3000 K. The effect of this variation is shown in Fig. 8: the lower flame temperature has almost no effect on erosion rate (if compared with the effect of propellant composition), and it only affects the surface temperature.

It is evident from Figs. 6–8 and from the previous discussion that the erosion rate shows a strong correlation with the concentration of oxidizing species whereas the flame temperature has almost no influence on surface recession. However, if the flame temperature is low enough, then the recession process may be strongly influenced by chemical kinetics, and one may find a large effect of nozzle material reactivity as well as of flame temperature. Relatively low flame temperatures, in fact, may result in nozzle surface temperatures of about 2000–2500 K where the influence of chemical kinetics can be very pronounced, hence causing the diffusion-limited model to overestimate recession. As shown in Fig. 7, the propellant with the lowest content of aluminum exhibits a wall temperature distribution that crosses the 2500 K limiting value. This would explain the overestimate of the erosion rate shown in Table 3: the error introduced by the diffusion-limited approximation is negligible (less than 1%) for propellants with higher aluminum content, where diffusion processes control the erosion, and tend to increase as the aluminum content is decreased, where kinetics rates become important due to the lower surface temperatures. These results show that, for metallized propellants ensuring sufficiently high wall temperatures, a surface equilibrium assumption is a valid approximation and the obtained computations satisfactorily predict the experimental data.

As a final test, Fig. 9 shows the comparison of erosion rate and surface temperature for the metallized and nonmetallized propellant compositions shown in Table 1. Again, it can be noted that, even if the flame temperature of the metallized propellant (3500 K) is much higher than that of the nonmetallized propellant (3000 K), the erosion rate for the former is much lower than the latter. If one looks at the surface temperature profile of Fig. 9b, it can be seen that the predicted

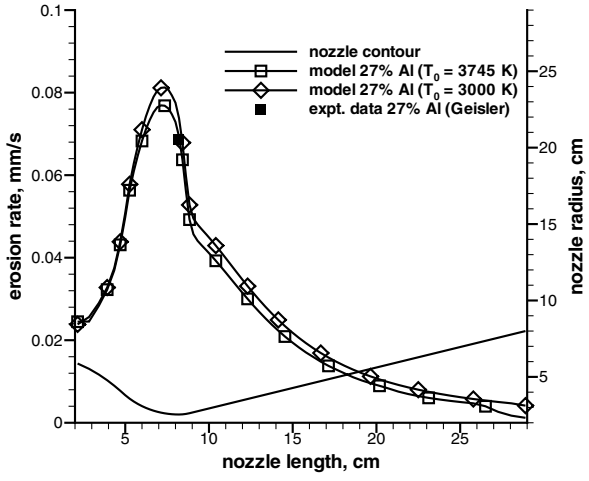

a) Erosion rate distribution (expt. data from [25])

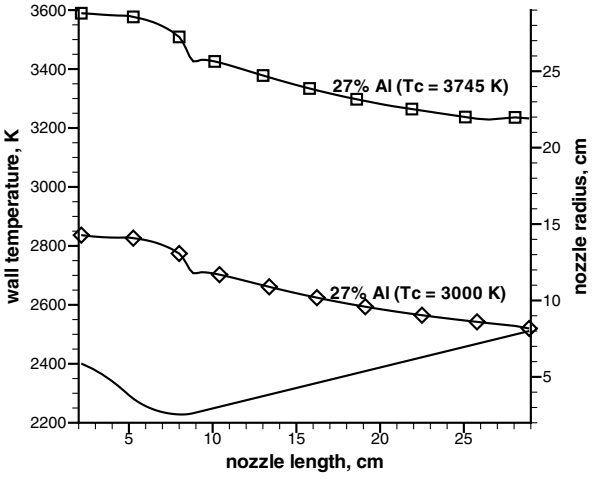

b) Wall temperature distribution

Fig. 8 Effect of flame temperature on erosion rate and wall temperature distribution.

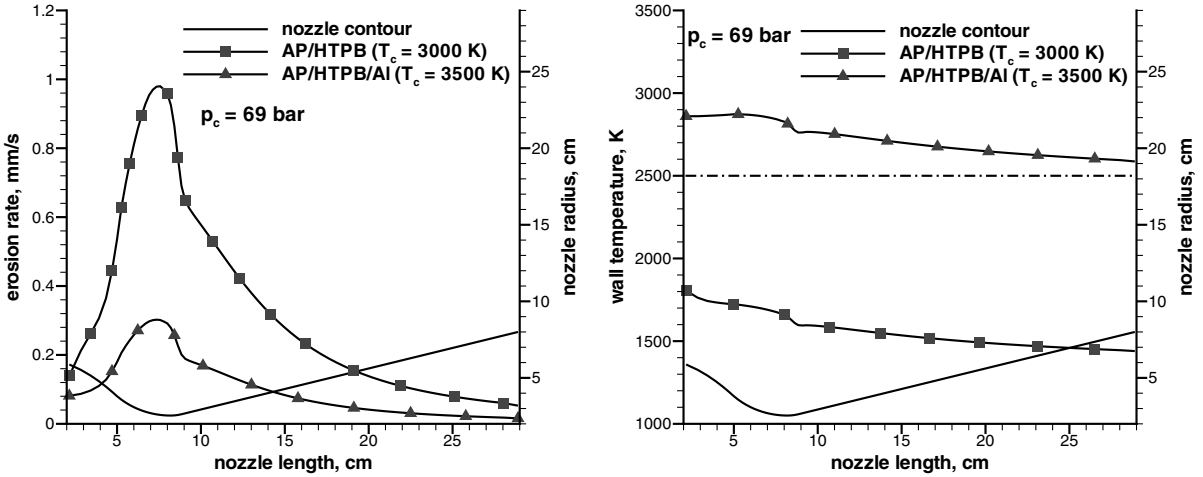

a) Erosion rate due to metallized and non-metallized propellants

b) Surface temperature due to metallized and non-metallized propellants

Fig. 9 Comparison of metallized and nonmetallized propellants.

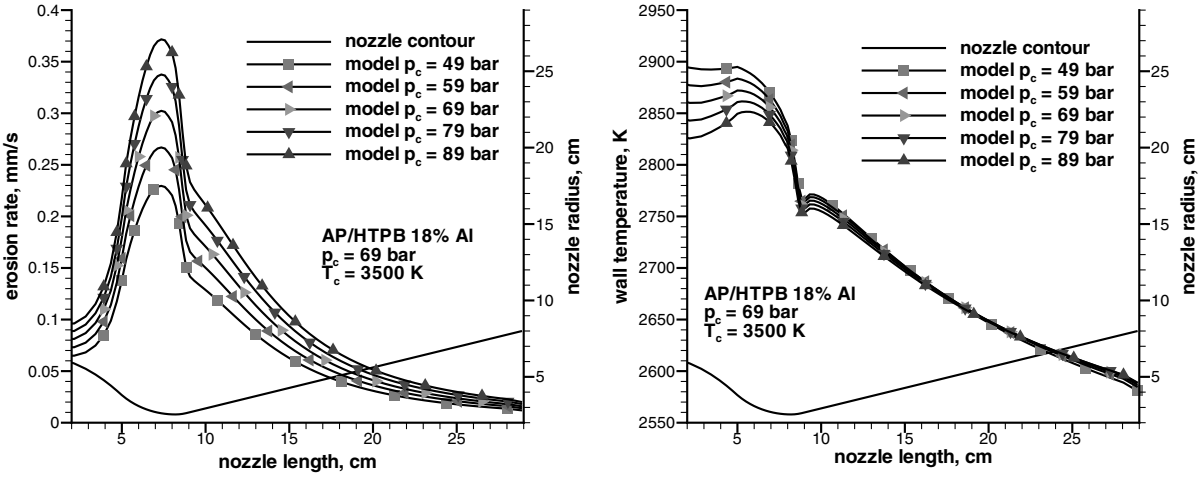

a) Erosion rate along the nozzle length

b) Surface temperature along the nozzle length

Fig. 10 Effect of chamber pressure on erosion rate and surface temperature.

surface temperature for the nonmetallized propellant is very low, less than 2000 K at the throat. Such a low temperature is presumably incorrect, because at low temperatures the erosion rate is expected to be kinetic-limited and, hence, the oxidizing species are not completely consumed at the surface. This would cause a reduction in the erosion rate and a consequent increase of the surface temperature due to slower surface reactions. The computed erosion rate for the nonmetallized propellant of Fig. 9a is more than 2.5 times that of the metallized propellant at the throat, being evidently an overestimate of the surface erosion rate.

C. Effect of Chamber Pressure

The preceding discussion has shown that the composition of the propellant plays an important role in determining the recession rate. Another important parameter is the chamber pressure [7,8,12,14]. The mass transfer rate of oxidizing species across the boundary layer to the nozzle surface is proportional to the gas-phase density and, consequently, to the pressure. Moreover, higher pressure results in higher Reynolds number, which enhances the transport mechanism.

The plotted results of Fig. 10a show that chamber pressure has a very strong influence on the recession rate. A change in the chamber pressure from 50 to 90 bar causes an increase in the recession rate of about 60%. Figure 10b shows the influence of chamber pressure on the surface temperature along the nozzle wall. Chamber pressure has a slight effect on surface temperature: higher pressures tend to

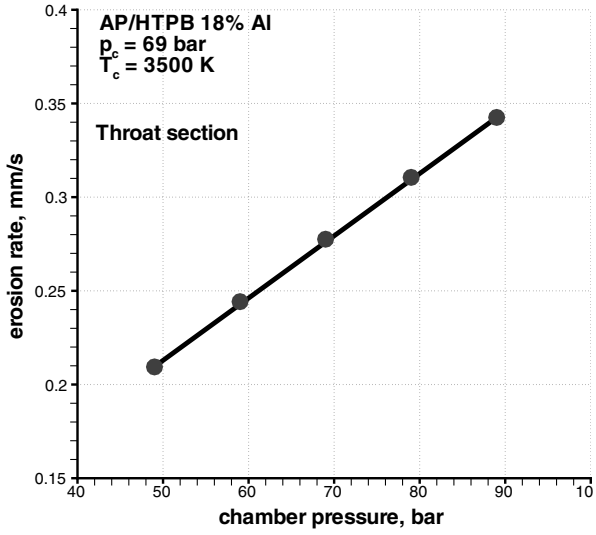

Fig. 11 Effect of chamber pressure on erosion rate at the nozzle throat.

decrease the surface temperature upstream of the throat and to increase it downstream of the throat. The effect, however, is very small. With other parameters remaining nearly constant, the linear dependence of the throat erosion rate on the motor operating pressure is clearly seen in Fig. 11. These results are in agreement with the experimental studies of Klager [7] showing that chamber pressure plays a significant role in the rate of recession, with recent studies showing that the recession rate increases almost linearly with pressure [12,14].

V. Conclusions

A general model based on a full Navier–Stokes approach is developed to examine thermochemical ablation of C/C heat protection materials in SRM environments. This problem is of critical importance to predict nozzle erosion rate and, hence, motor performance. The model includes all the relevant physics of the hot-gas flow, the ablation process, and the internal heat conduction into the material. The two regions, gas and solid, are fully coupled at the surface by appropriate energy and mass balances, allowing the surface conditions to be solved as part of the overall solution. The surface thermochemistry model is based on heterogeneous chemical equilibrium and can account for both surface oxidation and sublimation. Even if a surface nonequilibrium treatment is a more general approach, the present model permits a simplification in the problem formulation without limiting the model accuracy for many practical conditions. Indeed, the predicted surface recession rates show an excellent agreement with the available experimental data. The results show that the most important factors that dictate the erosion process are concentrations of the oxidizing species at the nozzle inlet, diffusion of oxidizing species toward the nozzle surface, and chamber pressure. Calculated results showed that oxidation of carbon to CO is the principal cause of nozzle recession. H_2O is the dominant oxidizing species, with CO_2 and OH being of secondary importance because their concentrations are about one order of magnitude lower than that of water vapor. The temperature and pressure conditions at wall are such that no surface sublimation is produced. Consistent with experimental results, the diffusion-limited recession rate shows an increase with increasing chamber pressure, exhibiting almost a linear correlation, although it is almost unaffected by chamber temperature. The erosion rate decreases with an increase in the aluminum content of the solid propellant, even though the flame temperatures increases. Results have also shown the limits of a diffusion-limited approach, which overestimate the erosion rate when the surface temperature drops below a limiting value where surface kinetics control the recession process.

Acknowledgment

This study has been partially supported by the Italian Ministry of University and Scientific Research.

References

[1] Swope, L. W., and Berard, M. F., "Effect of Solid-Rocket Propellant Formulations and Exhaust-Gas Chemistries on the Erosion of Graphite Nozzles," *AIAA Solid Propellant Rocket Conference*, AIAA, New York, Jan. 1964.

[2] Delaney, L. J., Eagleton, L. C., and Jones, W. H., "A Semiquantitative Prediction of the Erosion of Graphite Nozzle Inserts," *AIAA Journal*, Vol. 2, No. 8, 1964, pp. 1428–1433. doi:10.2514/3.2570

[3] McCuen, P. A., Schaefer, J. W., Lundberg, R. E., and Kendall, R. M., "A Study of Solid-Propellant Rocket Motor Exposed Materials Behavior," U.S. Air Force Rocket Propulsion Lab., Rept. AFRPLTR-65-33, Edwards AFB, CA, 1965.

[4] McDonald, A. J., and Hedman, P. O., "Erosion of Graphite in Solid-Propellant Combustion Gases and Effects on Heat Transfer," *AIAA Journal*, Vol. 3, No. 7, 1965, pp. 1250–1257. doi:10.2514/3.3117

[5] Lewis, J. C., Floyd, I. J., and Cowlard, F. C., "A Laboratory Investigation of Carbon-Gas-Reactions of Relevance to Rocket Nozzle Erosion," AGARD CP-52, Neuilly sur Seine, France, Feb. 1970.

[6] Tong, H., Hartman, G. J., Chu, E. K., and Murphy, A. J., "AFRPL Graphite Performance Prediction Program-Improved Capability for the Design and Ablation Performance Prediction of Advanced Air Force Solid Propellant Rocket Nozzles," U.S. Air Force Rocket Propulsion Lab., Rept. AFRPL-TR-76-70, Edwards AFB, CA, Dec. 1976.

[7] Klager, K., "The Interaction of the Efflux of Solid Propellants with Nozzle Materials," *Propellants and Explosives*, Vol. 2, No. 3, 1977, pp. 55–63. doi:10.1002/prep.19770020304

[8] Kuo, K. K., and Keswani, S. T., "A Comprehensive Theoretical Model for Carbon–Carbon Composite Recession," *Combustion Science and Technology*, Vol. 42, Nos. 3–4, 1985, pp. 145–164. doi:10.1080/00102208508960374

[9] Keswani, S. T., and Kuo, K. K., "Validation of an Aerothermochemical Model for Graphite Nozzle Recession and Heat-Transfer Processes," *Combustion Science and Technology*, Vol. 47, Nos. 3–4, 1986, pp. 177–192. doi:10.1080/00102208608923872

[10] Borie, V., Brulard, J., and Lengelle, G., "Aerothermochemical Analysis of Carbon–Carbon Nozzle Regression in Solid-Propellant Rocket Motors," *Journal of Propulsion and Power*, Vol. 5, No. 6, 1989, pp. 665–673. doi:10.2514/3.23204

[11] Geisler, R. L., "The Prediction of Graphite Rocket Nozzle Recession Rates," *The 1981 JANNAF Propulsion Meeting*, Chemical Propulsion Information Agency Publ. 342, May 1981, pp. 173–196.

[12] Thakre, P., and Yang, V., "Chemical Erosion of Carbon–Carbon/Graphite Nozzles in Solid-Propellant Rocket Motors," *Journal of Propulsion and Power*, Vol. 24, No. 4, 2008, pp. 822–833. doi:10.2514/1.34946

[13] Keswani, S. T., Andiroglu, E., Campbell, J. D., and Kuo, K. K., "Recession Behavior of Graphitic Nozzles in Simulated Rocket Motors," *Journal of Spacecraft and Rockets*, Vol. 22, No. 4, 1985, pp. 396–397. doi:10.2514/3.25763

[14] Acharya, R., and Kuo, K. K., "Effect of Pressure and Propellant Composition on Graphite Rocket Nozzle Erosion Rate," *Journal of Propulsion and Power*, Vol. 23, No. 6, 2007, pp. 1242–1254. doi:10.2514/1.24011

[15] Moyer, C. B., and Rindal, R. A., "An Analysis of the Chemically Reacting Boundary Layer and Charring Ablator. Part II: Finite Difference Solutions for the In-Depth Response of Charring Materials Considering Surface Chemical and Energy Balances," NASA CR 1061, 1968.

[16] Quan, V., "Quasi-Steady Solution for Ablation-Erosion Heat Transfer," *Journal of Spacecraft and Rockets*, Vol. 7, No. 3, 1970, pp. 355–357. doi:10.2514/3.29938

[17] Bianchi, D., Nasuti, F., Martelli, E., and Onofri, M., "A Numerical Approach for High-Temperature Flows over Ablating Surfaces," AIAA Paper 2007-4537, 2007.

[18] Bianchi, D., "Modeling of Ablation Phenomena in Space Applications," Ph.D. Dissertation, Univ. of Rome "La Sapienza", Rome, Jan. 2008.

[19] Martelli, E., "Studio della Fluidodinamica Interna di Ugelli Propulsivi di Tipo Dual Bell," Ph.D. Dissertation (in Italian), Univ. of Rome "La Sapienza", Rome, Jan. 2006.

[20] Nasuti, F., and Onofri, M., "Analysis of Unsteady Supersonic Viscous Flows by a Shock Fitting Technique," *AIAA Journal*, Vol. 34, No. 7, 1996, pp. 1428–1434. doi:10.2514/3.13249

[21] Moretti, G., "A Technique for Integrating Two-Dimensional Euler Equations," *Computers and Fluids*, Vol. 15, No. 1, 1987, pp. 59–75. doi:10.1016/0045-7930(87)90005-3

[22] Gordon, S., and McBride, B. J., "Computer Program for Calculation of Complex Chemical Equilibrium Compositions and Applications," NASA RP 1311, 1994.

[23] Spalart, P. R., and Allmaras, S. R., "A One-Equation Turbulence Model for Aerodynamic Flow," *La Recherche Aerospatiale : Bulletin Bimestriel de l'Office National d'Etudes et de Recherches Aerospatiales*, Vol. 1, 1994, pp. 5–21.

[24] Geisler, R. L., and Beckman, C. W., "The History of the BATES Motors at the Air Force Rocket Propulsion Laboratories," AIAA Paper 98-3981, 1998.

[25] Geisler, R. L., "The Relationship Between Solid Propellant Formulation Variables and Nozzle Recession Rates," *JANNAF Rocket Nozzle Technology Subcommittee Meeting*, JANNAF, July 1978.

T. Lin
Associate Editor